# Simulation of Heat Transfer Characteristics in Channel with Square Rib Under Uniform and Turbulent Inlet Conditions

*LI Heng, YU Ting, WANG Duo, ZU Yingqing, XU Hongyi*[*]

Department of Aeronautics and Astronautics, Fudan University, Shanghai 200433, P. R. China

**Abstract:** The detailed flow structures and closely-related heat transfer characteristics are investigated along the wall of a cooling channel with rib tabulator by computation. Three typical Reynolds numbers defined by the rib height are set at 200, 500, 1 300, and the Mach numbers is 0.2, respectively. Two inlet boundary conditions, including the uniform and the fully-developed turbulent conditions, are used to study the turbulence effects on the characteristics of heat transfer in the vicinity of rib and wall. Results show that the local Nusselt number increases when the Reynolds number rises from 200 to 1 300. At lower Reynolds number, the turbulent inlet condition generates more tangible heat transfer enhancement. At higher Reynolds number, however, the uniform inlet condition contributes more to the convective heat transfer effects. The paper discovers that the high Nusselt number has a consistent correlation with the positive and negative sign alteration of the shear layer on the wall, which satisfactorily explains the mechanisms of heat transfer enhancement due to the flow.

**Key words:** convective heat transfer; turbulent inflow condition; rortex method; shear layer

## 0 Introduction

To improve the heat transfer efficiency in a cooling channel of turbine blade in modern aero-engine, some wall structures, such as protuberances or pin-fins, were popularly used to increase the heat transfer areas in the devices. On the other hand, the fields of velocity and temperature are affected by these structures, making the convective heat transfer more efficient. Therefore, it is important to give the data of the velocity and thermal fields near the wall.

Recently, Fouladi et al.[1] experimentally investigated the flow and convective heat transfer on a flat plate with a square rib at four typical Reynolds numbers. Compared with the smooth plate, heat transfer is significantly enhanced in the ribbed plate.

Several numerical simulations were conducted to obtain more detailed information of rib flows.

Heat transfer and flow in a single-rib mounted channel were investigated by Miura et al.[2-3]. All cases used the fully-developed turbulent inlet conditions. They found that, the mean Nusselt number on the ribbed wall was about 1.3 times larger than the one on a smooth wall. Single rib mounted on the wall was concluded as a useful technique for heat-transfer enhancement[2]. Besides, it was found that the fully-developed turbulence in the separated shear layer correlated well with the higher Nusselt number. Therefore, they concluded that the high performance of heat transfer in the ribbed channel was attributed to the mechanisms of the induced strong fluctuation[2]. Besides, riblet surface structures were also investigated[4].

Due to the fact that most of the previous simulations were based on an incompressible model, the paper considers the compressibility of fluids by solving the compressible Navier-Stokes equations,

which is more accurate to reflect the density varia-tions in real flows. In fact, the temperature differ-ences are remarkable between the cooling fluid and the hot turbine blade surface, and therefore the den-sity variations of cooling gas are significant near the hot wall even if the Mach number is not very high. Hence, it is more valid to accurately resolve the den-sity and temperature fields with the current densi-ty-based compressible algorithm. In addition, the paper also investigated the effects of inlet turbulence on the heat transfer by comparing the uniform and fully-developed turbulent inflows. Particularly, the next generation of vortex identification method[5] is applied to this papaer to analyze the phenomena of vortical flow structures and their effects on the heat transfer. The flow configuration of cooling channel with a rib tabulator is considered and the Navi-er-Stokes equations are solved in its two dimension-al form. Detailed thermal flow fields are investigated and some strongly-coupled flow and heat transfer phenomena are analyzed.

# 1 Mathematical Model and Governing Equations

The non-dimensionalized Navier-Stokes equa-tions for compressible fluid are written in Cartesian coordinate as

$$\frac{\partial U}{\partial t} + \frac{\partial F}{\partial x} + \frac{\partial G}{\partial y} = \frac{\partial F_v}{\partial x} + \frac{\partial G_v}{\partial y} \qquad (1)$$

$$U = \begin{bmatrix} \rho \\ \rho u \\ \rho v \\ E_t \end{bmatrix}, F = \begin{bmatrix} \rho u \\ \rho u^2 + p \\ \rho uv \\ u(E_t + p) \end{bmatrix}, G = \begin{bmatrix} \rho v \\ \rho uv \\ \rho v^2 + p \\ v(E_t + p) \end{bmatrix}$$

$$F_v = \begin{bmatrix} 0 \\ \tau_{xx} \\ \tau_{xy} \\ u\tau_{xx} + v\tau_{xy} + k\frac{\partial T}{\partial x} \end{bmatrix}$$

$$G_v = \begin{bmatrix} 0 \\ \tau_{yx} \\ \tau_{yy} \\ u\tau_{yx} + v\tau_{yy} + k\frac{\partial T}{\partial y} \end{bmatrix} \qquad (2)$$

$$\tau_{xx} = -\frac{2}{3} \mu \left( \frac{\partial u}{\partial x} + \frac{\partial v}{\partial y} \right) + 2\mu \frac{\partial u}{\partial x} \qquad (3)$$

$$\tau_{yy} = -\frac{2}{3} \mu \left( \frac{\partial u}{\partial x} + \frac{\partial v}{\partial y} \right) + 2\mu \frac{\partial v}{\partial y} \qquad (4)$$

$$\tau_{xy} = \mu \left( \frac{\partial u}{\partial y} + \frac{\partial v}{\partial x} \right)$$

$$\tau_{yx} = \tau_{xy} \qquad (5)$$

where $\rho$ denotes density. $u$ and $v$ are the velocity components in $x$ and $y$ Cartesian directions, respec-tively. $p$ and $T$ represent pressure and temperature. $\mu$ and $k$ are molecular viscosity coefficient and ther-mal conductivity, respectively. $E_t$ is the total energy defined as $\rho(c_v T + (u^2 + v^2)/2)$, and $C_v$ is the spe-cific heat at constant volume .

All above parameters are nondimensional vari-ables defined as

$$\begin{cases} x = \dfrac{x'}{L_{ref}} \\ y = \dfrac{y'}{L_{ref}} \\ \rho = \dfrac{\rho'}{\rho_\infty} \end{cases}, \begin{cases} u = \dfrac{u'}{U_\infty} \\ v = \dfrac{v'}{U_\infty} \\ T = \dfrac{T'}{T_\infty} \end{cases}, \begin{cases} p = \dfrac{p'}{\rho_\infty U_\infty^2} \\ t = \dfrac{U_\infty t'}{L_{ref}} \\ \mu = \dfrac{\mu'}{\mu_\infty} \end{cases} \qquad (6)$$

where the superscript symbol ($'$) represents a primi-tive parameter in its dimensional form, and the sub-script symbol ($\infty$) denotes dimensional reference variable such as the quantity at inlet. $L_{ref}$ is the refer-ence length. In the paper, the rib height $e$ is the ref-erence length $L_{ref}$. The ideal gas equation of state is given by

$$p = \rho RT \qquad (7)$$

where $R$ is the specific gas constant, and above equation can be reduce to

$$p = \frac{\rho T}{\gamma Ma^2} \qquad (8)$$

where $\gamma$ is the ratio of specific heat and $Ma$ is the Mach number. The Reynolds number is defined as

$$Re = \frac{\rho_\infty U_\infty L_{ref}}{\mu_\infty} \qquad (9)$$

The spatial derivatives in convective terms were discretized with the third-order MUSCL scheme[6-7], and the spatial derivatives in viscous term were solved with forth-order centered finite-dif-ference scheme. The third-order TVD Runge-Kutta scheme[8] was used in time advancement. The com-putational codes are developed based on the above methods.

## 2　Computational Parameters and Solution Conditions

### 2.1　Computational parameters

To study the turbulence effects on the heat-transfer performance, the uniform and fully-developed turbulent inlet conditions are used at three typical Reynolds numbers defined by rib height, $Re = 200, 500, 1\,300$. As shown in Table 1, the Mach number and Prandtl number are set at 0.2 and 0.71.

The non-dimensional time step $\Delta t$ is given at $2.0 \times 10^{-4}$ to satisfy the Courant-Friedrich-Levy (CFL) condition. The turbulence statistics are accumulated up to $1.0 \times 10^{6}$ time steps.

**Table 1　Computational parameters.**

| Case | $Re$ | $Ma$ | $Pr$ | Grid | $\Delta y^{+}$ | Inlet conditions |
|---|---|---|---|---|---|---|
| Case 1 | 200 | 0.2 | 0.71 | 428×262 | 0.325 | Uniform |
| Case 2 | 200 | 0.2 | 0.71 | 428×262 | 0.325 | Fully-developed turbulent |
| Case 3 | 500 | 0.2 | 0.71 | 428×262 | 0.350 | Uniform |
| Case 4 | 500 | 0.2 | 0.71 | 428×262 | 0.350 | Fully-developed turbulent |
| Case 5 | 1 300 | 0.2 | 0.71 | 428×262 | 0.414 | Uniform |
| Case 6 | 1 300 | 0.2 | 0.71 | 428×262 | 0.414 | Fully-developed turbulent |

The grid resolutions are measured by $\Delta y^{+}$, which is defined as $\Delta y^{+} = \Delta y u_{\tau}/v$, where $\Delta y$ is the distance of the first point away from the wall, and $v$ is the kinematic viscosity coefficient. The local friction velocity $u_{\tau}$ is defined as

$$u_{\tau} = \sqrt{\frac{\tau_{w}}{\rho_{w}}} \qquad (10)$$

where $\rho_{w}$ is the fluid density nearest the wall, and $\tau_{w}$ is the wall shear stress defined as

$$\tau_{w} = \mu_{w} \left( \frac{\partial u}{\partial y} \right)_{w} \qquad (11)$$

where $\mu_{w}$ and $(\partial u/\partial y)_{w}$ are the molecular viscosity coefficient and the normal velocity gradient nearest the wall. The grid resolutions, based on the local friction velocity $u_{\tau}$, meet the condition of a maximum of $\Delta y^{+} < 0.5$ along the $x$ direction. The local Nusselt number is defined as

$$Nu = -\frac{H}{T_{w} - T_{b}} \frac{\partial T}{\partial n} \qquad (12)$$

where $T_{w}$ is the wall temperature, $T_{b}$ the bulk mean temperature, and $\partial T/\partial n$ the normal temperature gradient on the wall.

### 2.2　Boundary conditions

For the no-slip wall, a ghost-cell immersed boundary method[9-10] is used in the paper with the Dirichlet boundary condition is applied and the fluid velocity on the wall is set equal to zero. On the wall, the normal pressure gradient is zero and then the density can be obtained by the perfect-gas state equation. For the inlet, uniform incoming flow conditions or fully-developed turbulent conditions are applied. For the outlet, the backpressure is set to the environmental pressure and all other variables are based on the zero gradient condition in streamwise direction, namely, the Neumann boundary condition.

### 2.3　Computational grid generation

Fig.1 shows the computational domain and the Cartesian coordinate system. The channel dimensions are $L = 42e$ and $H = 10e$. A square rib with a distance $L_{1} = 11e$ is set at the wall of channel. The temperature at no-slip wall is kept as 1.5 and the incoming flow temperature is 1.0.

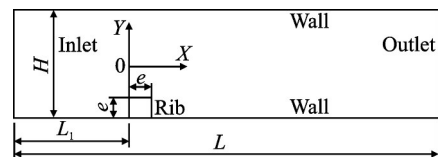The grids are refined towards the channel and rib walls. Such a grid arrangement is used in order



Fig.1　Computational domain and coordinate system

to accurately resolve the boundary layers near the walls.

# 3 Validation and Grid‑Dependency Study

## 3. 1 Model validation

In order to validate present flow model and code, a classical case of the flow over a fixed circular, is studied. The computational domain is $20D \times 10D$, where $D$ is the cylindrical diameter. The Reynolds number based on $D$ is set at 40 and 1 000. The grid number is $600 \times 600$ in $x$ and $y$ directions and the grid resolution is chosen to satisfy $\Delta x \approx \Delta y \approx 1/150D$ near the cylindrical wall.

Fig.2 shows the cylindrical surface pressure coefficient defined as $C_p = (p - p_\infty)/(1/2\rho U_\infty^2)$. From the comparison, it can be seen that the good agreements are obtained between the present results and the reference data given by Luo, et al.[9] and Ghais, et al.[11].
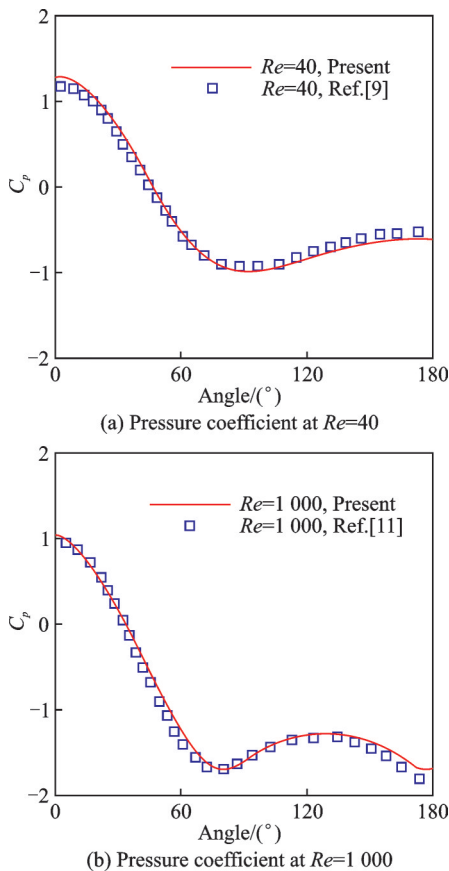
## 3. 2 Grid dependence study

The simulations are performed on three levels of coarse, medium and fine grids in $y$ direction, as shown in Table 2. Similarly, the computations are implemented on medium and fine grids in $x$ direction.

**Table 2 Four grid arrangements**

| Case | Grid |
| --- | --- |
| Case 1 | $324 \times 262$ |
| Case 2 | $324 \times 133$ |
| Case 3 | $324 \times 520$ |
| Case 4 | $428 \times 262$ |

Fig. 3 shows that no significant difference is found between the medium and fine grids in $x$ direction. Similarly, there is no significant difference between the medium and fine grids in $y$ direction. Therefore, as a compromise of the grid resolution and computational work, all present studies are conducted on the fine grid in $x$ direction and on the medium grid in $y$ direction.
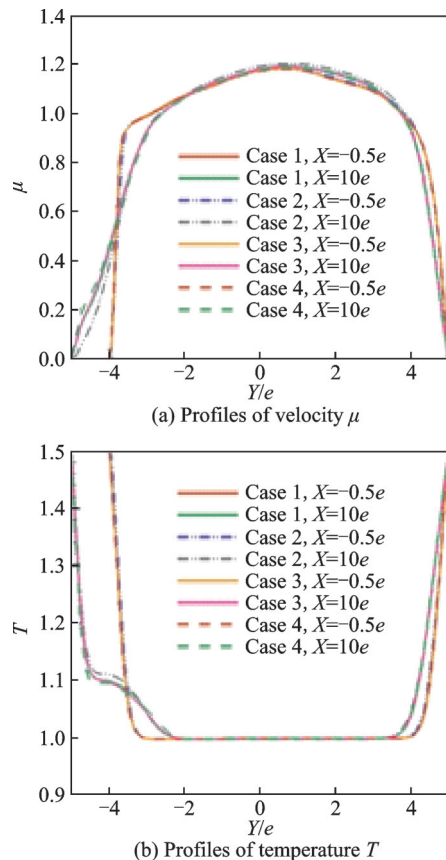


(a) Pressure coefficient at $Re$=40

(b) Pressure coefficient at $Re$=1 000

Fig.2　Comparison of pressure coefficient $C_p$



(a) Profiles of velocity $\mu$

(b) Profiles of temperature $T$

Fig.3　Comparison of velocity $u$ and temperature $T$ between coarse, medium and fine grids

# 4    Result Analyses and Discussions

## 4. 1    Time-averaged characteristics with uniform and fully-developed turbulent inflows

The turbulence fluctuations play a vital role for the downstream flow. Therefore, a fully-developed turbulence in a channel was resolved by a separated Direct Numerical Simulation[12]. The instantaneous turbulence data along a line inside the channel are extracted out and are imposed onto the inlet of the channel with a rib at present cases.

The re-attached point locations are determined based on the average streamwise velocity. For the first-layer grid point nearest the lower wall, the signs of velocity of $u$ are contrary on the both sides of the re-attached point. Therefore, we determine the re-attached point location based on the signs of streamwise velocity.

At lower Reynolds number of $Re=200$ with the turbulent inlet condition, the Nusselt number increases slowly, and reaches the peak value around the location of $11e$.

At lower Reynolds number($Re=200$) with the uniform inflow, the phenomena are similar. Compared with turbulent inflow, however, the Nusselt number increases slowly, and the peak is pushed further back to a distance of about $19e$ location (Fig. 4 (a) ). Compared with turbulent inflow, the maximum of local Nusselt number is a little smaller with uniform inflow, which is attributed to the smaller temperature gradient near reattached point. As shown in Fig.4(b), the location of $Nu/Nu_0>1$ is near at $X=8e$ for the case with turbulent inlet, while it is near at $X=13e$ for the case with uniform inlet. In Fig.4(b), $Nu$ and $Nu_0$ are the local Nusselt numbers on rib-wall and smooth wall. Overall, the turbulent inlet provides more significant heat-transfer effects compared with the uniform inflow.

At medium Reynolds number ($Re=500$) with the turbulent inlet condition, as shown in Fig.5, the Nusselt number increases rapidly, and reaches its peak at a location around $X=8e$. Compared with the case of $Re=200$, the current case has a small-

er-sized wake vortices. As the separated region is reduced, the averaged Nusselt number is larger, and the overall heat transfer is more effective than that on the smooth wall. From Fig.5, it can be seen that the present results coincide well with the data from Miura et al. [2-3]. Please note that the equivalent Reynolds number based on rib height is 455 in the computation given by Miura et al.[2-3]. Besides, the reattaching length is similar to the experimental data[3,14], as shown in Table 3.

At medium Reynolds number ($Re=500$) with the uniform inlet, as shown in Fig.5, the trend of the Nusselt number is similar to the case with the turbulent inlet. However, the peak is larger and is pushed further back to a location around $10e$ in Fig.5 (a). Besides, compared with turbulent inflow, the maximum of local Nusselt number is larger with uniform inflow, which is attributed to the larger temperature gradient near the reattached point. As shown in Fig.5(b), the location of $Nu/Nu_0>1$ is near at $X=4e$ for the case with turbulent inlet, while it is near at $X=5.5e$ for the case with uniform inlet. But, the maximum of $Nu/Nu_0$ is larger for the case with the uniform inlet. Overall, compared with the turbulent inlets, the uniform inlets provide more significant average heat transfer effects.

At high Reynolds number ($Re=1\,300$) with the turbulent inlet condition (Fig. 6 ), the Nusselt number increases rapidly, with a local peak at around $X=1.5e$ and then reaches the maximum at around $X=5e$.

At high Reynolds number ($Re=1\,300$) with the uniform inlet condition (Fig.6), the trend of the Nusselt number is similar to the case with the turbulent inlet condition. However, the peak is larger and the peak location is more forward downstream at around $4.2e$ location (Fig. 6 (a) ). Compared with turbulent inflow, the maximum of local Nusselt number is larger with uniform inflow, which is attributed to the larger temperature gradient near the reattached point. As shown in Fig.6(b), the location of $Nu/Nu_0>1$ is near at $X=1.1e$ for the two case. While, the maximum of $Nu/Nu_0$ is larger for the case with the uniform inlet. Overall, compared with the turbulent inlet conditions, the uniform inlet
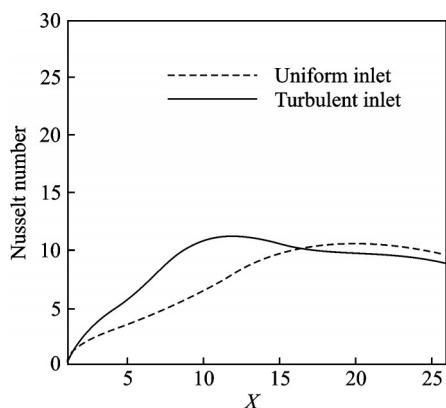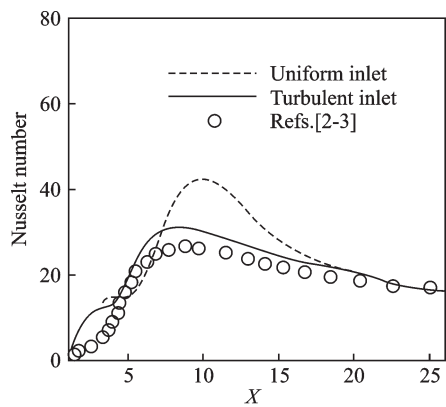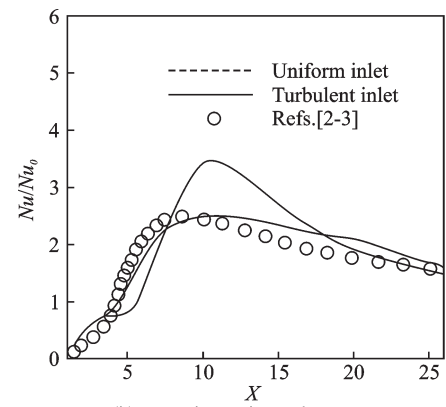
(a) Bottom wall
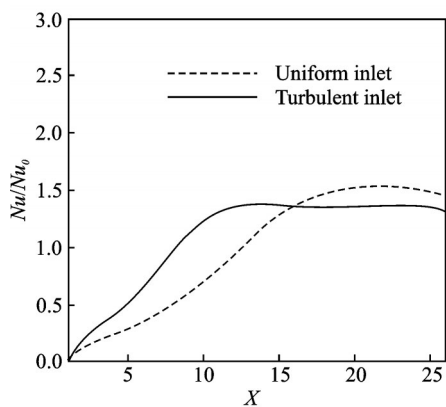


(b) Nusselt number enhancement $Nu/Nu_0$
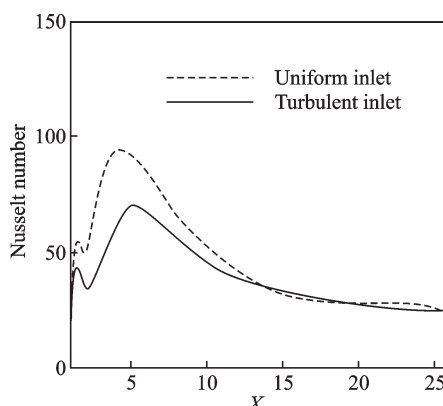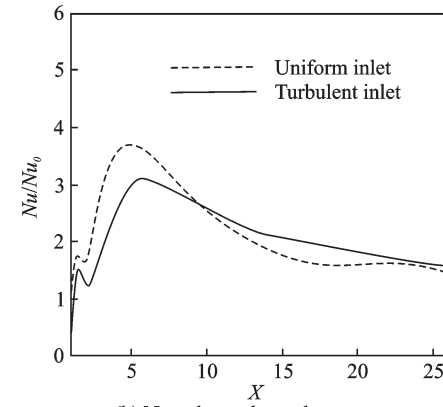
Fig.4    Local Nusselt number of $Re=200$

Table 3    Summary of the present reattaching length with the turbulent inlet conditions

| Authors | $Re$ | $L/e$ |
|---|---|---|
| Present | 200 | 9.5 |
| Miura et al.[3] | 475 | 7.0 |
| Present | 500 | 7.2 |
| Ali et al.[14] | 1 175 | 7.2 |
| Present | 1 300 | 5.0 |
| Ali et al.[14] | 3 390 | 5.5 |



(a) Bottom wall



(b) Nusselt number enhancement

Fig.6    Local Nusselt number of $Re=1\ 300$



(a) Bottom wall



(b) Nusselt number enhancement

Fig.5    Local Nusselt number of $Re=500$

conditions generate the more effective heat transfer effects.

Figs. 7—9 show the mean temperature contours and stream lines at $Re=200$, 500 and 1 300. There is a larger-sized stabilized eddy behind the rib in Fig. 7. However, there are two vortices behind the rib at $Re=1\ 300$, including a small and a large one, as shown in Fig.9.

Generally, at low Reynolds number ($Re=200$), the turbulent inlet provides more significant heat transfer effects. At medium Reynolds number ($Re=500$) and at higher Reynolds number ($Re=1\ 300$), the uniform inlet conditions provide more
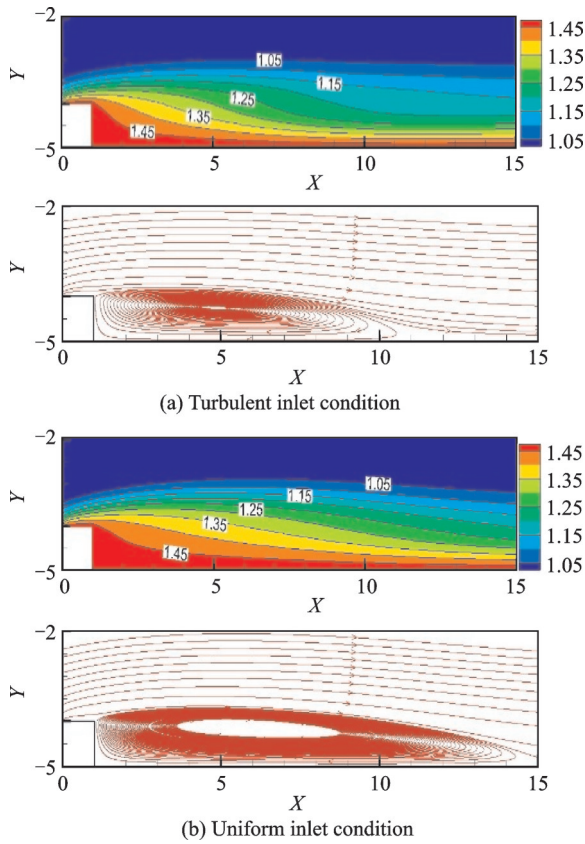
(a) Turbulent inlet condition



(b) Uniform inlet condition

Fig.7    Mean temperature contours and stream lines at $Re=200$



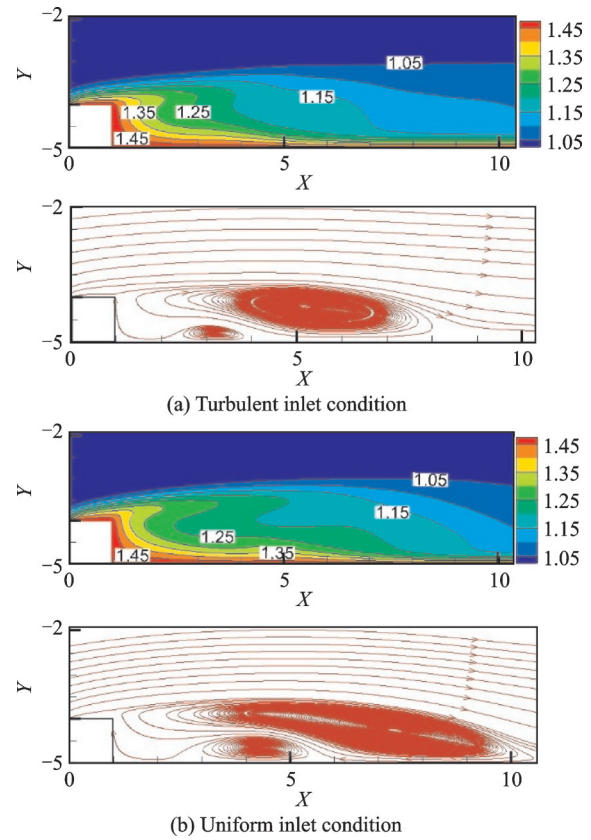(a) Turbulent inlet condition



(b) Uniform inlet condition

Fig.8    Mean temperature contours and stream lines at $Re=500$

significant heat transfer effects.

Generally, with the increase of Reynolds number, the separated region decreases and the reattachment length becomes shorter. This qualitative conclusion can be found in previous data[14]. As shown in Tables 3, 4, the reattaching length decreases from $9.5e$ to $5.0e$ with the increase of Reynolds number from 200 to 1 300, which coincides well with the experimental data[14] and the numerical results[3]. Those phenomena of wake region variation are connected with the convective heat transfer behind rib. With the Reynolds number increases, the wake becomes smaller. As a result, the local Nusselt number peak increases near the reattachment point and the overall heat transfer effects are enhanced. Please note that all the reference data used here are based on the equivalent Reynolds number defined with rib height, and the reattaching length is computed from $X=1$ to re-attached point location.

## 4. 2    Structures of instantaneous field

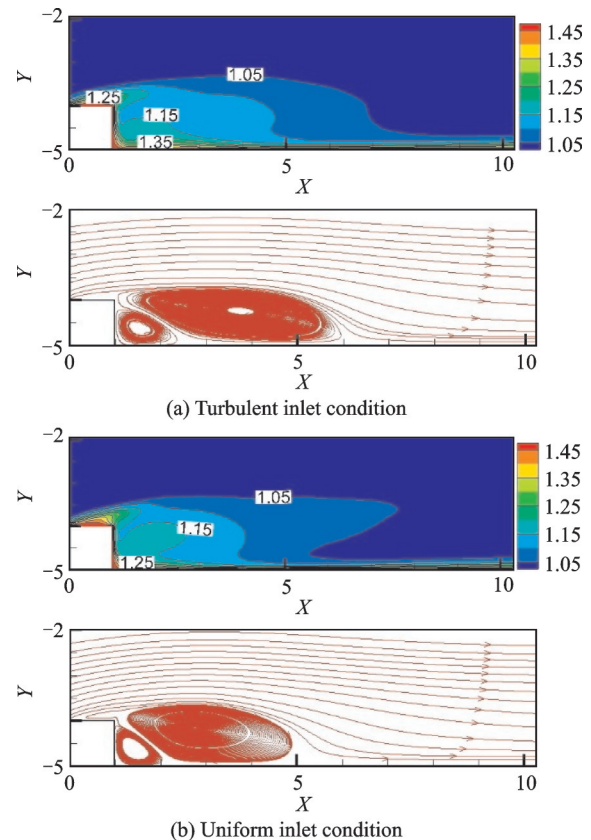In order to further understand the convective



(a) Turbulent inlet condition



(b) Uniform inlet condition

Fig.9    Mean temperature contours and stream lines at $Re=1\ 300$

**Table 4    Summary of the reattaching length with two inlet conditions**

| Inlet condition | $Re$ | $L/e$ |
| --- | --- | --- |
| Turbulent | 200 | 9.5 |
| Uniform | 200 | 14.0 |
| Turbulent | 500 | 7.2 |
| Uniform | 500 | 9.5 |
| Turbulent | 1 300 | 5.0 |
| Uniform | 1 300 | 4.0 |

heat transfer, the turbulent structures are analyzed. Traditional methods of the vortice identification, such as vorticity method[15], $Q$-criterion[16] and $\lambda_2$-criterion[17], are commonly used. Recently, a novel and more precise approach named as Rortex method was presented by Liu et al.[5,18]. To precisely identify the vortex, the main idea of this method is that, the vorticity vector $\nabla \times v$ is decomposed into a rotational vector $R$ which is called the Rortex and a non-rotational vector $S$ representing the shear effect

$$\nabla \times v = R + S \qquad (13)$$

where the rotational vector $R$ is defined as

$$R = R \cdot r \qquad (14)$$

where $r$ indicates the rotational axes of vortices, and $R$ presents the magnitude of rotational vector. The definitions of $R$ can refer to Liu, et al.[5,18].

In Refs.[5,18], the mathematical definition of Rortex were provided and the validations were conducted based on the late-transition DNS data of semi-flat plate, which well presented the effectiveness of Rortex function in representing the characteristics of vortical flow. Therefore, the paper is based on Rortex to analyze the vortical structures and the its effects on the convective heat transfer on the ribbed wall.

There, the typical cases with the turbulent inlet at $Re=500$ are illustrated. After the fields are fully developed, the evolutionary process of rotational vector and non-rotational vector are extracted with dimensionless time interval $\Delta t=6$, as shown in Fig.10.
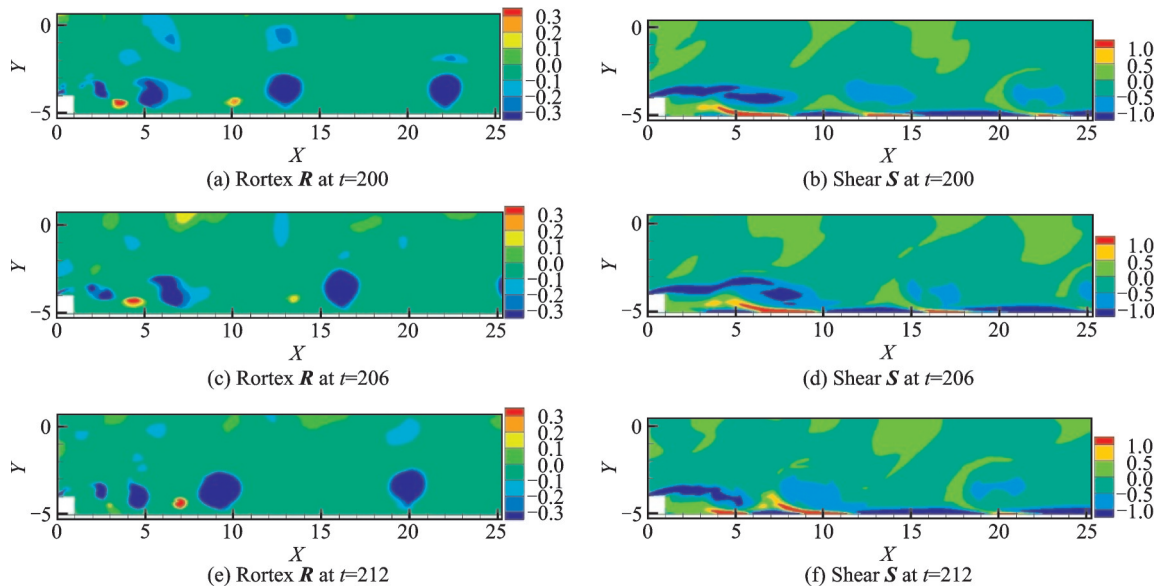


(a) Rortex $R$ at $t=200$

(b) Shear $S$ at $t=200$

(c) Rortex $R$ at $t=206$

(d) Shear $S$ at $t=206$

(e) Rortex $R$ at $t=212$

(f) Shear $S$ at $t=212$

Fig.10    Evolution of rortex $R$ and shear $S$ at $Re=500$ with turbulent inlet condition

The magnitude of Rortex variable $R$ represents the vortex strength, as shown in Figs.10(a, c, e). As the time evolving, several small-scale vortices are generated on the upper side of rib. With a strong shear near the top surface of rib, those small-scale vortices starte shedding and evolve into the more intensive large-scale eddies, as shown in Fig.10. Particularly, the counter-rotating tail vortices indicated

by the red region in Figs.10(a, c, e) are observed downstream. It is noteworthy that the counter-rotating eddies are generated, strengthened and then gradually weakened, eventually disappeared downstream.

Besides, the prominent strong shear along the upper edge of the separated region and along the channel wall are observed in Figs.10(b, d, f). From

a time-sequential frame of the shear variable $S$, it can be seen that the distinctive positive and negative shear regions alternate when evolving downstream along the wall. Specifically，after a distance of $3e$ behind the rib，the strong shear banded regions are alternatively changed，which well explains the phenomenon of strong heat transfer effects.

Several cases are extracted to find out the correlation between the high heat transfer characteristics and the alternation of positive and negative shear regions. The shear $S$ is extracted in the case of $Re=$ 200 with turbulent inlet condition. As shown in Fig.11，there are alternations of positive and negative shear regions after the location of $X=8$. Similarly，at higher Reynolds number of $Re=1\ 300$ with turbulent inlet condition，the shear $S$ is shown in
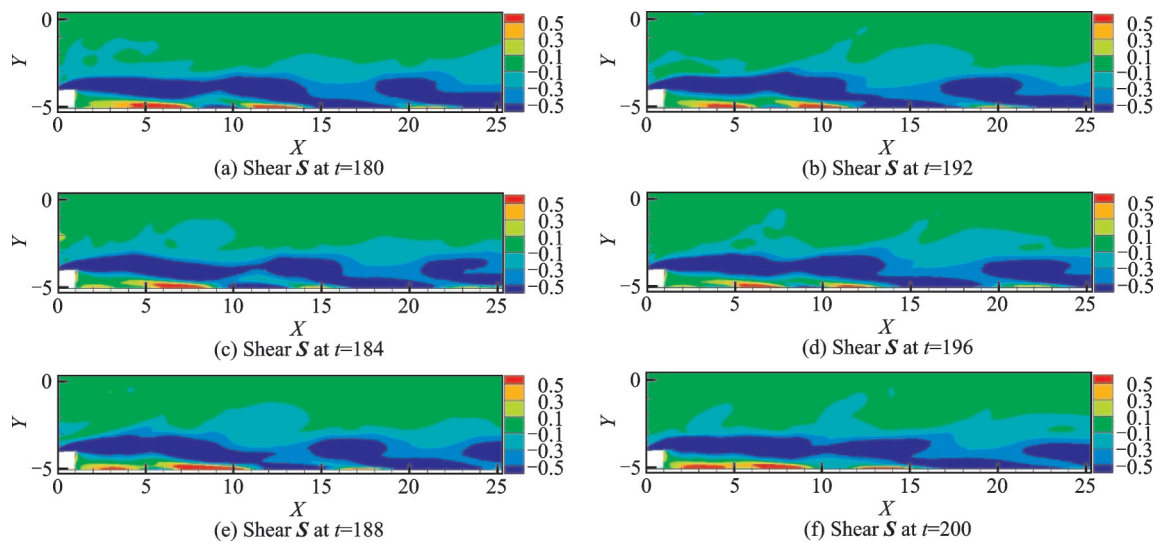
Fig.12. It is obvious that the positive and negative shear regions alternate after the rib，especially for the region of $1<X<10$，where the Nusselts number is larger (as shown in Fig.6).

Another case of $Re=500$ with uniform inlet condition is extracted to further confirm the conclusion that the high heat transfer characteristics are relevant with the alternations of positive and negative shear regions. As shown in Fig.13，for the region of $7<X<15$ where $Nu$ number is larger (as shown in Fig.5)，the positive and negative shear regions alternate. Therefore，it is reasonable to conclude that the alternate regions of the positive and negative shear layer on the wall are consistent with the locations of high Nusselt number.



Fig.11　Evolution of shear $S$ at $Re=200$ with turbulent inlet condition

## 5　Conclusions

The paper investigates the convective heat transfer on the channel wall attached with a square-shape rib by resolving the two-dimensional Navier-Stokes equations. Two types of inlet boundary conditions，including the uniform and the fully-developed turbulent conditions，are applied to study the turbulence effects on the characteristics of heat transfer in the vicinity of rib and wall. The study is conducted at three typical Reynolds numbers of $Re=200$，500，1 300，respectively. Some important conclusions are summarized in the following：

(1) With the increase of $Re$ from 200 to 1 300，the local $Nu$ increases and the overall heat transfer effects are enhanced. Compared with smooth wall，the ratios $Nu/Nu_0$ are also increased with the increase of $Re$.

(2) At lower Reynolds number ($Re=200$)，the turbulent inlet conditions give more effective heat transfer results than the uniform inlet conditions. The turbulent inlet boundary conditions provide stronger disturbance. The separated regions are smaller than the case of the uniform inlet. Accordingly，the local $Nu$ peak positions are advanced，
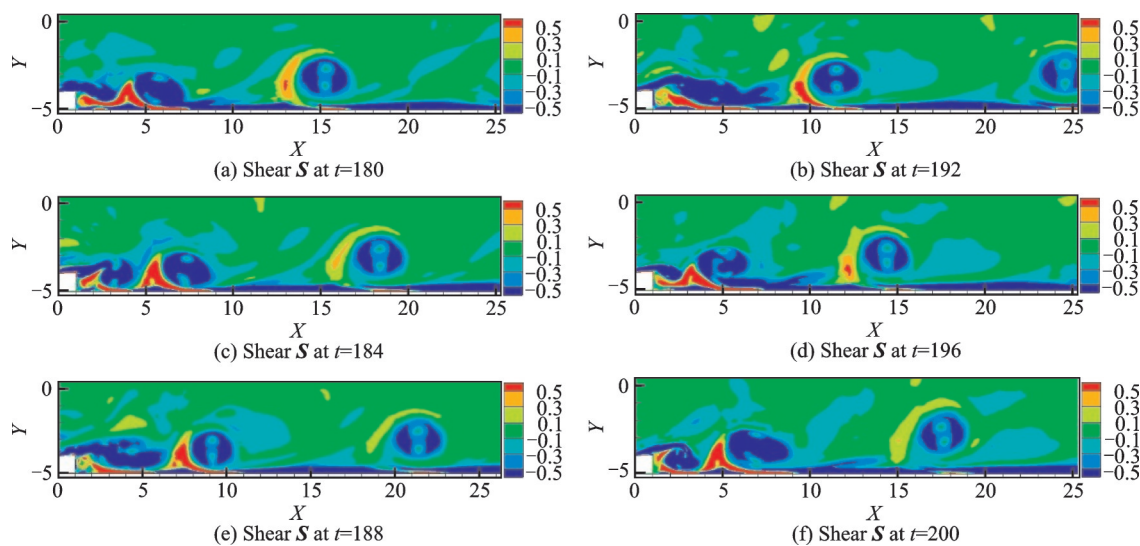
Fig.12   Evolution of shear $S$ at $Re=1\,300$ with turbulent inlet condition
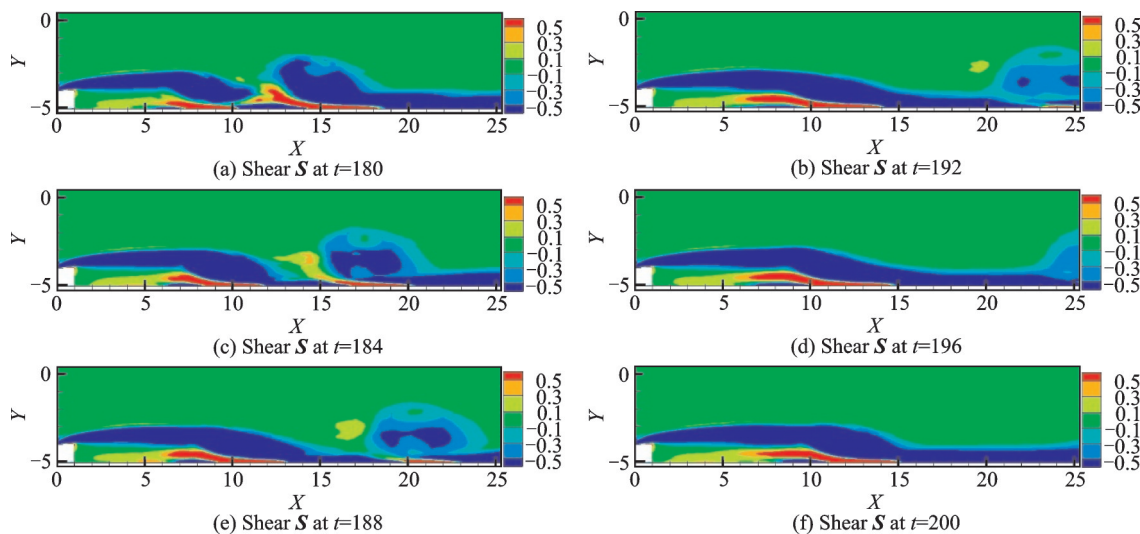


Fig.13   Evolution of shear $S$ at $Re=500$ with uniform inlet condition

and the overall heat transfer effects are enhanced.

(3) At higher Reynolds number ($Re=1\,300$), the uniform inlet conditions give more effective heat transfer results than the turbulent inlet conditions. Smaller wake eddy regions are observed. In the uniform inlet conditions, the local Nusselt number peak value is larger and the overall heat transfer effects are better than those in the case with turbulent inlet conditions.

(4) Based on the instantaneous field of vortices evolvement, vortices appear near the top surface of the rib with strong shear effects. Then the vortices shed and their intensities increase downstream. Particularly, the alternate regions of the positive and negative shear layer on the wall are consistent with the locations of high Nusselt number.

## References

[1]   FOULADI F, HENSHAW P, TING S K, et al. Flat plate convection heat transfer enhancement via a square rib [J]. International Journal of Heat and Mass Transfer, 2017, 104: 1202-1216.

[2]   MIURA T, MATSUBARA K, SAKURAI A. Heat transfer characteristics and Reynolds stress budgets in single-rib mounting channel [J]. Journal of Thermal Science & Technology, 2010, 5(5): 135-150.

[3]   MIURA T, MATSUBARA K, SAKURAI A. Turbulent-heat-flux and temperature-variance budgets in a single-rib mounting channel [J]. Journal of Thermal Science and Technology, 2012, 7(1): 120-134.

[4]   FENG B B, CHEN D R, WANG J D, et al. Drag reducing and increasing mechanism on triangular riblet

surface [J]. Transactions of Nanjing University of Aeronautics and Astronautics, 2014, 31(1): 78-84.

[5] LIU C Q, GAO Y S, TIAN S L, et al. Rortex—A new vortex vector definition and vorticity tensor and vector decompositions [J]. Physics of Fluids, 2018, 30(3): 035103.

[6] LEER B V. Towards the ultimate conservative difference scheme. V. A second-order sequel to Godunov's method [J]. Journal of Computational Physics, 1979, 32(1): 101-136.

[7] COLELLA P, A direct Eulerian MUSCL scheme for gas dynamics [J].SIAM Journal on Scientific & Statistical Computing, 1982, 6(1): 104-117.

[8] SHU C W. Total-variation-diminishing time discretizations [J]. SIAM Journal on Scientific & Statistical Computing, 1988, 9(6): 1073-1084.

[9] LUO K, ZHUANG Z Y, FAN J R, et al. A ghost-cell immersed boundary method for simulations of heat transfer in compressible flows under different boundary conditions [J]. International Journal of Heat & Mass Transfer, 2016, 92: 708-717.

[10] LUO K, MAO C L, ZHUANG Z Y, et al. A ghost-cell immersed boundary method for the simulations of heat transfer in compressible flows under different boundary conditions Part-II: Complex geometries [J]. International Journal of Heat & Mass Transfer, 2017, 104: 98-111.

[11] GHIAS R, MITTAL R, DONG H. A sharp interface immersed boundary method for compressible viscous flows [J]. Journal of Computational Physics, 2007, 225(1): 528-553.

[12] XU H Y. Direct numerical simulation of turbulence in a square annular duct [J]. Journal of Fluid Mechanics, 2009, 621: 23-57.

[13] ALI M S, TARIQ A, GANDHI B K. Detailed investigation on rib turbulated flow inside a rectangular duct [C]// ASME 2012 International Mechanical Engineering Congress and Exposition. [S.l.]: ASME, 1259-1271.

[14] ALI M S, TARIQ A, GANDHI B K. Flow and heat transfer investigation behind trapezoidal rib using PIV and LCT measurements [J]. Experiments in Fluids, 2013, 54(5): 1-15.

[15] WU J Z, MA H Y, ZHOU M D. Vorticity and vortex dynamics [M]. Berlin, Heidelberg: Springer, 2006.

[16] HUNT J C R, WRAY A A, MOIN P. Eddies, streams, and convergence zones in turbulent flows [C]//Proceeding of the Summer Program in Center for Turbulence Research. [S.l.]:[s.n.],193-208.

[17] JEONG J, HUSSAIN F. On the identification of a vortex [J]. Journal of Fluid Mechanics, 1995, 285: 69-94.

[18] LIU C Q, WANG Y Q, YANG Y, et al. New omega vortex identification method[J]. Science China Physics, Mechanics & Astronomy, 2016, 59(8): 684711.

**Authors**  Dr. **LI Heng** received B.S degree in Nanjing University of Science and Technology. Now, he is studying as a Ph.D. student in Fudan University. His research interest is the turbulence and heat transfer.

Dr. **YU Ting** received B.S degree in Shanghai University and M.S degree in Loughborough University. Now, he is studying as a Ph.D. student in Fudan University. His research interest is the turbulence and heat transfer.

Dr. **WANG Duo** received B.S degree in Shandong University and M.S degree in Loughborough University. Now, he is studying as a Ph.D. student in Fudan University. His research interest is the turbulence and heat transfer.

Prof. **ZU Yingqing** received Ph.D. degree in Energy & Sustainability from the University of Nottingham. He is now an associate professor at Fudan University. His research interest is single- and multi- phase fluid flow and heat transfer.

Prof. **XU Hongyi** received the Ph.D. degree in Queen's University of Canada. He is now a professor at Fudan University. As the Shanghai Thousand Talents, he has always been interested in the research of turbulence and heat transfer.

**Author contributions**    Dr. **LI Heng** developed the procedure and conducted the computations. Dr. **YU Ting** provided the initial computational grids and the inlet turbulent data. Dr. **WANG Duo** developed the physical model. Prof. **ZU Yingqing** provided guidance for the algorithm and the server. Prof. **XU Hongyi** provided guidance for the algorithm of immersed boundary technology and carefully revised this paper.

**Competing interests**    The authors declare no competing interests.

(Production Editor: Sun Jing)